Imaging Agents Hot Paper

International Edition: DOI: 10.1002/anie.201502287
German Edition: DOI: 10.1002/ange.201502287

Cartilage-Specific Near-Infrared Fluorophores for Biomedical Imaging**

Hoon Hyun, Eric A. Owens, Hideyuki Wada, Andrew Levitz, GwangLi Park, Min Ho Park, John V. Frangioni, Maged Henary, and Hak Soo Choi**

Abstract: *A novel class of near-infrared fluorescent contrast agents was developed. These agents target cartilage with high specificity and this property is inherent to the chemical structure of the fluorophore. After a single low-dose intravenous injection and a clearance time of approximately 4 h, these agents bind to all three major types of cartilage (hyaline, elastic, and fibrocartilage) and perform equally well across species. Analysis of the chemical structure similarities revealed a potential pharmacophore for cartilage targeting. Our results lay the foundation for future improvements in tissue engineering, joint surgery, and cartilage-specific drug development.*

Healthy cartilage is essential for a good quality of life. Its functions include cushioning joints and intervertebral spaces, giving form to the ears and nose, and protecting the trachea. All three histological types of cartilage, namely hyaline (articular when on a joint surface), elastic, and fibrocartilage, are produced by chondrocytes, or more precisely chondroblasts, until entrapment within their own extracellular matrix.[1–3] The three types differ mainly in the relative amounts of collagen, proteoglycans, and elastin present.

Cartilage dysfunction leads to several acute and chronic morbidities. In degenerative joint disease (DJD, osteoarthritis), destruction of cartilage on the articular surfaces of joints leads to pain and debilitation. DJD affects over 27 million patients in the USA alone and results in huge economic losses.[4] Because cartilage cannot regenerate like bone, replacement therapy through tissue engineering, and pharmacological treatment that prevents destruction are being intensely explored. However, even if these therapies existed tomorrow, there would be no way to assess pharmacological treatment noninvasively or to guide surgery for neo-cartilage transplantation.

Despite its high importance, cartilage is difficult to image. So far, most efforts to image and quantify cartilage have focused on magnetic resonance imaging (MRI),[1,5] however, the water-deficient composition of cartilage makes it a poor target for MRI.[6] Low X-ray absorption also makes cartilage a relatively poor target for clinical computed tomography (CT), and when using conventional microCT, it is essentially invisible.[7] There was a single-photon emission computed tomography (SPECT) radiotracer for cartilage reported in 2001,[8] namely ^{99m}Tc-labeled *N*-(triethylammonium)-3-propyl-[15]ane-N5, but no clinical studies have followed and recently published preclinical studies show poor image quality.[9]

To date, there isn't a single optical contrast agent for cartilage, and certainly not one in the near-infrared (NIR) wavelength range of 700–900 nm. NIR light has certain key advantages for biomedical imaging, including relatively low tissue absorption, reduced scatter, and minimal autofluorescence.[10–12] Thus, unlike visible light, which only penetrates a few hundred microns below a tissue surface, NIR light can penetrate millimeters to centimeters into living tissue. Therefore, the use of NIR fluorophores, that is, molecules that convert one NIR wavelength into another, permits a high signal-to-background ratio (SBR) to be produced.[12]

Initial in vivo screening of a large (> 300 unique chemical entities) NIR fluorophore library revealed a class of compounds with apparent specificity for cartilage. As shown in Scheme 1, a series of these molecules, along with several derivatives, was resynthesized from a pentamethine core for 700 nm fluorescence and a heptamethine core for 800 nm fluorescence (see the Supporting Information). The physicochemical and optical properties of the NIR fluorophores are summarized in Table 1. By modulating the nonresonant side chains of the polymethine core, the final NIR fluorophores could be systematically altered to tune the hydrophobicity,

[*] Prof. H. Hyun,[+] Dr. H. Wada, G. Park, Prof. M. H. Park, Prof. J. V. Frangioni, Prof. H. S. Choi
Division of Hematology/Oncology, Department of Medicine
Beth Israel Deaconess Medical Center and Harvard Medical School
330 Brookline Avenue, SL436A, Boston, MA 02215 (USA)
E-mail: hchoi@bidmc.harvard.edu

E. A. Owens,[+] A. Levitz, Prof. M. Henary
Department of Chemistry, Center for Diagnostics and Therapeutics
Georgia State University, Atlanta, GA 30303 (USA)
E-mail: mhenary1@gsu.edu

Prof. H. Hyun[+]
Department of Biomedical Sciences
Chonnam National University Medical School
Gwangju 501-746 (South Korea)

Prof. M. H. Park
Department of Surgery, Chonnam National University Medical School, Gwangju 501-746 (South Korea)

Prof. J. V. Frangioni
Curadel, LLC, 377 Plantation Street, Worcester, MA 01605 (USA)

Prof. H. S. Choi
Department of Cogno-Mechatronics Engineering
Pusan National University, Busan 609-735 (South Korea)

[+] These authors contributed equally to this work.

[**] This study was supported by the following grants from the National Institutes of Health: NIBIB grants no. R01-EB-010022 and no. R01-EB-011523. Dr. Frangioni is currently CEO of Curadel, LLC, which has licensed FLARE technology from the BIDMC. We thank David Burrington, Jr. for editing, and Eugenia Trabucchi for administrative assistance.

Supporting information for this article is available on the WWW under http://dx.doi.org/10.1002/anie.201502287.

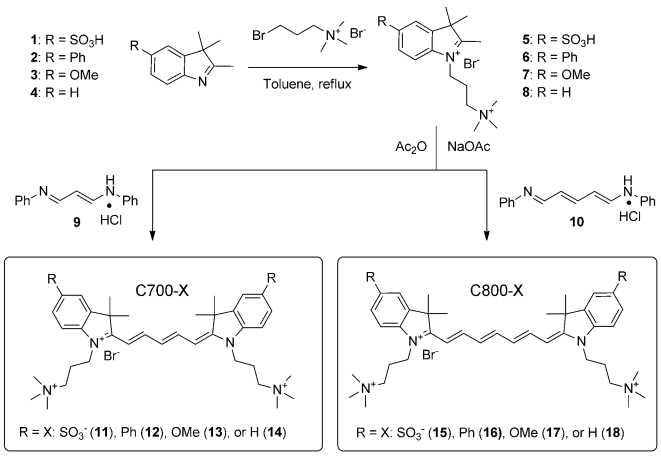

Scheme 1. Synthesis of the C700 and C800 NIR fluorophores.

Table 1: Physicochemical and optical properties of the C700 and C800 NIR fluorophores. Theoretical calculations of the molecular properties were calculated by using Marvin and JChem calculator plugins. All optical measurements were performed at 37 °C in 100% FBS buffered with 50 mM HEPES, pH 7.4.

700 nm Fluorophores	C700-SO3 (**11**)	C700-Ph (**12**)	C700-OMe (**13**)	C700-H (**14**)
molecular weight [Da]	713.97	655.98	615.91	555.86
Log *D* at pH 7.4	−2.20	−2.63	−4.93	−4.61
total polar surface Area (Å^2)	120.65	6.25	24.71	6.25
extinction coefficient [M^{-1} cm^{-1}]	85 000	131 000	96 500	110 400
absorbance maximum [nm]	650	691	666	646
emission maximum [nm]	668	716	692	665
Stokes shift [nm]	18	25	26	19
quantum yield [%]	11.5	12.4	9.7	10.8
800 nm Fluorophores	**C800-SO3 (15)**	**C800-Ph (16)**	**C800-OMe (17)**	**C800-H (18)**
molecular weight [Da]	740.01	682.01	641.95	581.90
Log *D* at pH 7.4	−1.67	−2.10	−4.40	−4.08
total polar surface area [Å^2]	120.65	6.25	24.71	6.25
extinction coefficient [M^{-1} cm^{-1}]	128 000	179 000	121 000	101 000
absorbance maximum [nm]	765	800	770	745
emission maximum [nm]	788	818	804	767
Stokes shift [nm]	23	18	34	22
quantum yield [%]	10.4	10.8	11.5	7.2

polarity, and electron-resonance properties without affecting the emission wavelength in the range of 650–800 nm. These wavelengths minimize tissue autofluorescence and maximize the fluorescence signal.[13]

As a preliminary in vivo test for cartilage targeting, C700 and C800 NIR fluorophores were intravenously injected into CD-1 mice (10 nmol; 0.4 mg kg^{-1}). The mice were imaged after 4 h and the fluorescent signals in the costal cartilage tissues were respectively quantified (Figure 1).

Interestingly, C700-OMe and C800-OMe showed the highest signal-to-background ratio (SBR, calculated from the difference in fluorescence intensity between costal cartilage and neighboring muscle) values compared to the other molecules, and both C700-H and C800-H also showed high cartilage uptake. Although the synergistic effects of the methoxy groups on the cationic polymethine structure for efficient cartilage binding are not well understood, methoxy groups improve the hydrophilicity (Log *D* at pH 7.4 < −4.0) and increase the polar surface area (24.71 Å). By contrast, the addition of sulfonates or phenyl groups to the polymethine backbone diminished the cartilage specificity of the final fluorophores. C700-Ph and C800-Ph showed high nonspecific background signals because of their increased hydrophobicity and unbalanced 3D conformation (data not shown), whereas the net surface charges of C700-SO3 and C800-SO3 were geometrically balanced between sulfonates and quaternary ammonium groups, thus resulting in no cartilage uptake. Furthermore, the polarity values for the sulfonated fluorophores are close to 120 Å^2, which is consistent with poor permeability of cell membranes.[14] Based on these results, we propose the pharmacophore shown in Scheme 2 for carti-

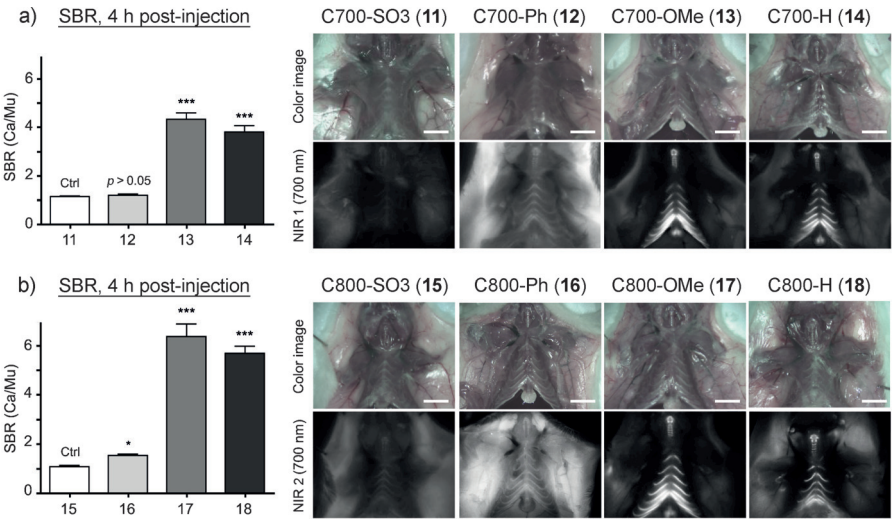

Figure 1. In vivo cartilage targeting with C700 (a) and C800 (b) NIR fluorophores in mice. Each fluorophore was injected intravenously into 25 g CD-1 mice (10 nmol; 0.4 mg kg^{-1}) 4 h prior to imaging. The SBR (Ca/Mu) was calculated from the fluorescence intensity of costal cartilage tissues versus the signal intensity of neighboring muscle obtained over the imaging period ($n = 3$, mean ± SD). *$p < 0.05$, ***$p < 0.001$. All NIR fluorescence images have identical exposure and normalization. Ca: cartilage, Mu: muscle. Scale bars = 1 cm.

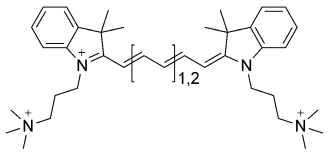

Scheme 2. Proposed pharmacophore for high-specificity cartilage binding in vivo.

lage binding. Unfortunately, we do not as yet know the molecular target for binding. Once this is known, it should be possible to further refine the pharmacophore.

Because C700-OMe and C800-OMe showed the highest SBR for cartilage tissues among the different derivatives tested, we selected these methoxy-substituted NIR fluorophores for further in vivo study. To determine whether cartilage type (hyaline, elastic, or fibrocartilage) affected uptake, we imaged all the major cartilage tissues at 4 h post-injection with C700-OMe and C800-OMe in CD-1 mice (Figure 2). After a single intravenous injection of each agent, all cartilage tissues were clearly visualized, including ears/nose, knee joints, costal cartilages, and intervertebral discs. Since the compositions of each cartilage tissue are different, we further performed histological evaluations with Alcian blue and hematoxylin and eosin (H&E) staining. As shown in Figure 2, Alcian blue (dark blue staining) mainly stained acidic glycosaminoglycans (GAGs) in cartilage, where strong NIR fluorescence was also observed. The histology data also confirm binding of our NIR fluorophores to all three types of cartilage. Since cartilage tissues are all produced by chondrocytes (or more precisely chondroblasts) and differ mainly in the relative amounts of collagen, proteoglycans, and elastin present, we believe that the molecules we developed must be binding either to the surface of chondrocytes, or more likely, to a secreted molecule with a high local concentration. Interestingly, the growth (epiphyseal) plate (Figure 2B, green arrows) was targeted along with the fibrocartilage of the knee joint in the young mice (8 weeks) used for the study. A major component of the growth plate is hyaline cartilage located in the metaphysis at each end of the long bones. Because the plate is typically found in children and adolescents, the results suggest that our NIR fluorophores can even bind to cartilage in early developmental stages.

Finally, we exploited the dual-NIR-channel capability of the FLARE imaging system to highlight cartilage and bone tissues simultaneously in real time. Since bone-targeting NIR fluorophores (e.g., P800SO3) have been previously developed by our group,[15] the combination of C700-OMe (emitting at 700 nm) and P800SO3[15] (emitting at 800 nm) was tested by injecting both agents together into mice and pigs. As shown in Figure 3, cartilage tissues were identified by C700-OMe in the 700 nm channel, whereas bone tissues were visualized with P800SO3 in 800 nm channel. This approach might prove useful in future tissue engineering studies, in which transplanted neocartilage could be visualized in one NIR channel and either bone or blood vessels could be visualized in the other. During human surgery, these new imaging agents might prove useful for estimating cartilage thickness during arthroscopy, or for finding inconspicuous damage to joints.

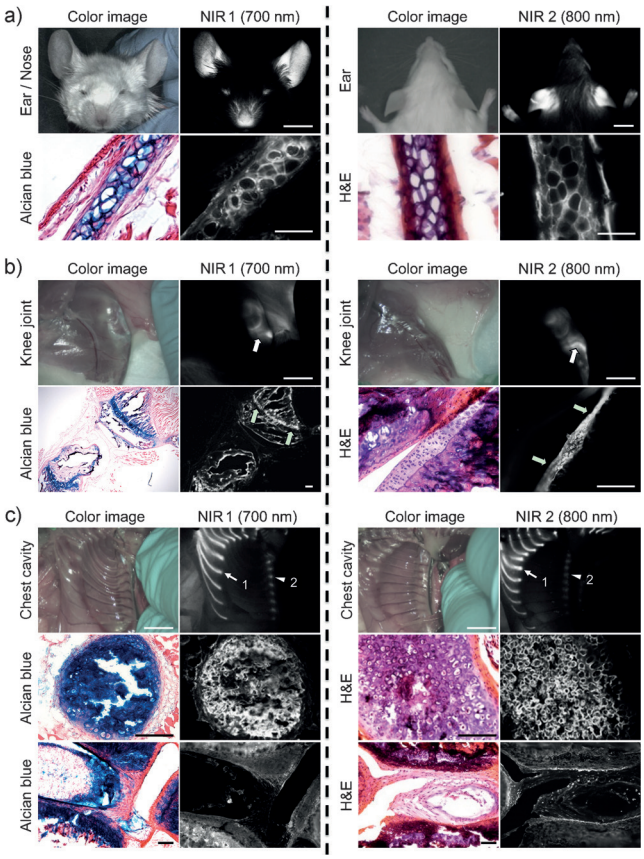

Figure 2. In vivo NIR imaging and histological analysis of cartilage tissues from ear (a), knee joint (b), and thoracic cavity (c) in mice. C700-OMe and C800-OMe were intravenously injected into 25 g CD-1 mice (10 nmol; 0.4 mg kg^{-1}) 4 h prior to imaging. The green arrows in (b) indicate the of the growth plates. The white arrows labelled 1 and the white arrowheads labelled 2 in (c) indicate hyaline and fibrocartilage, respectively. Alcian blue, H&E, and NIR images of resected cartilage tissues were obtained from the same animal. All NIR fluorescence images for each condition have identical exposure times and normalizations. Scale bars = 1 cm (for in vivo images) and 100 μm (for histology images). The images shown are representative of $n = 3$ independent experiments.

Along with endocrine-gland-specific[16] and bone-specific NIR fluorophores,[15] the novel cartilage-specific NIR fluorophores described herein are a third example of "structure-inherent targeting", in which tissue-/organ-specific targeting is engineered directly into the nonresonant structure of a NIR fluorophore, thus creating the most compact possible optical contrast agent for biomedical imaging. We hope that our present findings will lay the foundation for improved diagnosis and treatment of cartilage diseases.

Experimental Section

Synthesis of C700 and C800 NIR fluorophores: All chemicals and solvents were of American Chemical Society grade or HPLC purity. Starting materials were purchased from Sigma–Aldrich (Saint Louis, MO) and Fisher Scientific Inc. (Pittsburgh, PA) and used without purification. The reactions were followed by using reversed-phase silica-gel thin-layer chromatography plates (Merck EMD Millipore,

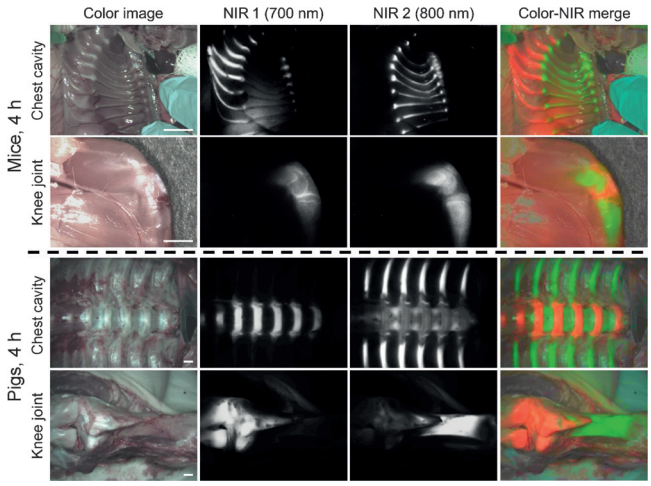

Figure 3. Dual-channel in vivo fluorescence imaging of cartilage and bone tissues with C700-OMe and P800SO3[15] in the same animal. C700-OMe and P800SO3 were co-injected intravenously into either 25 g CD-1 mice (top; 0.4 mg kg^{-1}) or 35 kg Yorkshire pigs (bottom; 0.02 mg kg^{-1}), 4 h prior to imaging. All NIR fluorescence images for each condition have identical exposure times and normalizations. Scale bars = 1 cm. Images are representative of $n = 3$ independent experiments. Pseudo-colored red and green colors were used for the 700 nm and 800 nm channels, respectively, in the color–NIR merged image.

Darmstadt, Germany) with 5% methanol in water as the mobile phase. Open column chromatography was utilized for the purification of all of the final compounds with reversed-phase silica gel (Dynamic Adsorbents, Norcross, GA). See the Supporting Information for detailed chemical syntheses and analyses.

Optical and physicochemical property analyses: All optical measurements were performed at 37 °C in 100% fetal bovine serum (FBS) buffered with 50 mM HEPES, pH 7.4. Absorbance and fluorescence emission spectra for the NIR fluorophores were measured by using fiber optic HR2000 absorbance (200–1100 nm) and USB2000FL fluorescence (350–1000 nm) spectrometers (Ocean Optics, Dunedin, FL). NIR excitations were provided by 5 mW of a 655 nm red laser pointer (Opcom Inc., Xiamen, China) and 8 mW of a 765 nm NIR laser diode light source (Electro Optical Components, Santa Rosa, CA) coupled through a 300 μm core diameter, NA 0.22 fiber (Fiberguide Industries, Stirling, NJ). For fluorescence quantum yield (QY) measurements, oxazine 725 in ethylene glycol (QY = 19%)[17] and ICG in DMSO (QY = 13%)[18] were used as calibration standards, under conditions of matched absorbance at 655 and 765 nm, respectively. Calculations for surface molecular charge, the partition coefficient (LogD at pH 7.4), and the total polar surface area (TPSA) were performed by using Marvin and JChem calculator plugins (ChemAxon, Budapest, Hungary).

NIR fluorescence imaging system: The dual-NIR channel FLARE imaging system has been described in detail.[19,20] In this study, 4 mW cm^{-2} of 670 nm excitation and 11 mW cm^{-2} of 760 nm excitation were used with white light (400–650 nm) at 40000 lx. Color and NIR fluorescence images were acquired simultaneously with custom software at rates up to 15 Hz over a 15 cm diameter field of view. The imaging system was positioned at a distance of 18 inches from the surgical field. For each experiment, camera exposure times and image normalization were held constant.

Animal models: Animals were housed in an AAALAC-certified facility and were studied under the supervision of the BIDMC IACUC in accordance with approved institutional protocols (#101–2011 for rodents and #034–2013 for pigs). Male CD-1 mice (25–30 g, 8 weeks, Charles River Laboratories, Wilmington, MA) were anesthetized with 100 mg kg^{-1} ketamine and 10 mg kg^{-1} xylazine intraperitoneally (Webster Veterinary, Fort Devens, MA). Female Yorkshire pigs (E.M. Parsons and Sons, Hadley, MA) averaging 35 kg were induced with 4.4 mg kg^{-1} intramuscular Telazol (Fort Dodge Labs, Fort Dodge, IA), intubated, and maintained with 2% isoflurane (Baxter Healthcare Corp., Deerfield, IL). Following anesthesia, electrocardiograms, heart rate, pulse oximetry, and body temperature were monitored throughout surgery.

Quantitative analysis: At each time point, the fluorescence and background intensity of a region of interest (ROI) over each tissue was quantified by using custom FLARE software. The signal-to-background ratio (SBR) was calculated as SBR = fluorescence/background, where background is the signal intensity of neighboring tissues, such as muscle or skin, measured over the imaging period. All NIR fluorescence images for a particular fluorophore were normalized identically for all conditions of an experiment. At least three animals were analyzed at each time point. Statistical analysis was carried out by using the unpaired Student's *t*-test or one-way analysis of variance (ANOVA). Results were presented as mean ± SD and curve fitting was performed using Prism version 4.0a software (GraphPad, San Diego, CA).

Histology and NIR fluorescence microscopy: Cartilage tissues were placed in 2% paraformaldehyde in PBS for 30 min before mounting in Tissue-Tek OCT compound (Fisher Scientific, Pittsburgh, PA) and flash-freezing in liquid nitrogen. Frozen samples were cryosectioned (10 μm per slice), observed by NIR fluorescence microscopy, and also stained with Alcian blue or hematoxylin and eosin (H&E). NIR fluorescence microscopy was performed with a 4-filter Nikon Eclipse TE300 microscope system as previously described.[21,22] The microscope was equipped with a 100 W mercury light source (Chiu Technical Corporation, Kings Park, NY), NIR-compatible optics, and a NIR-compatible 10X Plan Fluor objective lens and a 100X Plan Apo oil immersion objective lens (Nikon, Melville, NY). Images were acquired on an Orca-AG (Hamamatsu, Bridgewater, NJ). Image acquisition and analysis was performed with iVision software (BioVision Technologies, Exton, PA). Two custom filter sets (Chroma Technology Corporation, Brattleboro, VT) composed of 650 ± 22 nm and 750 ± 25 nm excitation filters, 675 nm and 785 nm dichroic mirrors, and 710 ± 25 nm and 810 ± 20 nm emission filters were used to detect C700-OMe and C800-OMe signals, respsctively, in the frozen tissue samples.

Keywords: cartilage · fluorophores · imaging agents · NIR fluorescence · targeted dyes

How to cite: *Angew. Chem. Int. Ed.* **2015**, *54*, 8648–8652
Angew. Chem. **2015**, *127*, 8772–8776

[1] T. Irie, K. Oda, A. Shiino, M. Kubo, S. Morikawa, N. Urushiyama, S. Aonuma, T. Kimura, T. Inubushi, T. Oohashi, N. Komatsu, *MedChemComm* **2013**, *4*, 1508–1512.
[2] R. C. Stewart, P. N. Bansal, V. Entezari, H. Lusic, R. M. Nazarian, B. D. Snyder, M. W. Grinstaff, *Radiology* **2013**, *266*, 141–150.
[3] J. D. Freedman, H. Lusic, B. D. Snyder, M. W. Grinstaff, *Angew. Chem. Int. Ed.* **2014**, *53*, 8406–8410; *Angew. Chem.* **2014**, *126*, 8546–8550.
[4] L. Murphy, C. G. Helmick, *Orthop. Nurs.* **2012**, *31*, 85–91.
[5] C. Ding, Y. Zhang, D. Hunter, *Curr. Opin. Rheumatol.* **2013**, *25*, 127–135.
[6] M. D. Crema, F. W. Roemer, M. D. Marra, D. Burstein, G. E. Gold, F. Eckstein, T. Baum, T. J. Mosher, J. A. Carrino, A. Guermazi, *Radiographics* **2011**, *31*, 37–61.
[7] M. Z. Ruan, B. Dawson, M. M. Jiang, F. Gannon, M. Heggeness, B. H. Lee, *Arthritis Rheum.* **2013**, *65*, 388–396.
[8] M. Ollier, J. C. Maurizis, C. Nicolas, J. Bonafous, M. de Latour, A. Veyre, J. C. Madelmont, *J. Nucl. Med.* **2001**, *42*, 141–145.

[9] E. G. Miot-Noirault, J. A. Vidal, O. Gauthier, P. Auzeloux, J. Lesoeur, F. Cachin, S. Askienazy, J. M. Chezal, C. Vinatier, *Eur. J. Nucl. Med. Mol. Imaging* **2012**, *39*, 1169 – 1172.
[10] S. Achilefu, *Angew. Chem. Int. Ed.* **2010**, *49*, 9816 – 9818; *Angew. Chem.* **2010**, *122*, 10010 – 10012.
[11] H. Kobayashi, M. Ogawa, R. Alford, P. L. Choyke, Y. Urano, *Chem. Rev.* **2010**, *110*, 2620 – 2640.
[12] A. L. Vahrmeijer, M. Hutteman, J. R. van der Vorst, C. J. van de Velde, J. V. Frangioni, *Nat. Rev. Clin. Oncol.* **2013**, *10*, 507 – 518.
[13] J. H. Lee, G. Park, G. H. Hong, J. Choi, H. S. Choi, *Quant. Imaging Med. Surg.* **2012**, *2*, 266 – 273.
[14] S. H. Kim, G. Park, H. Hyun, J. H. Lee, Y. Ashitate, J. Choi, G. H. Hong, E. A. Owens, M. Henary, H. S. Choi, *Biomed. Mater.* **2013**, *8*, 014110.
[15] H. Hyun, H. Wada, K. Bao, J. Gravier, Y. Yadav, M. Laramie, M. Henary, J. V. Frangioni, H. S. Choi, *Angew. Chem. Int. Ed.* **2014**, *53*, 10668 – 10672; *Angew. Chem.* **2014**, *126*, 10844 – 10848.
[16] H. Hyun, M. H. Park, E. A. Owens, H. Wada, M. Henary, H. J. Handgraaf, A. L. Vahrmeijer, J. V. Frangioni, H. S. Choi, *Nat. Med.* **2015**, *21*, 192 – 197.
[17] R. Sens, K. H. Drexhage, *J. Lumin.* **1981**, *24*, 709 – 712.
[18] C. Benson, H. A. Kues, *J. Chem. Eng. Data* **1977**, *22*, 379 – 383.
[19] Y. Ashitate, S. H. Kim, E. Tanaka, M. Henary, H. S. Choi, J. V. Frangioni, R. Flaumenhaft, *J. Vasc. Surg.* **2012**, *56*, 171 – 180.
[20] S. Gioux, H. S. Choi, J. V. Frangioni, *Mol. Imaging* **2010**, *9*, 237 – 255.
[21] H. S. Choi, Y. Ashitate, J. H. Lee, S. H. Kim, A. Matsui, N. Insin, M. G. Bawendi, M. Semmler-Behnke, J. V. Frangioni, A. Tsuda, *Nat. Biotechnol.* **2010**, *28*, 1300 – 1303.
[22] H. S. Choi, B. I. Ipe, P. Misra, J. H. Lee, M. G. Bawendi, J. V. Frangioni, *Nano Lett.* **2009**, *9*, 2354 – 2359.

Received: March 11, 2015
Published online: June 10, 2015

